Experimental Study of Liquid Propellant Rotating Detonation Combustor

Shiro Ito[1], Kazuki Ishihara[1], Kentaro Yoneyama[1], Keisuke Goto[1], Noboru Itouyama[1], Hiroaki Watanabe[1], Akira Kawasaki[1], Ken Matsuoka[1], Jiro Kasahara[1], Akiko Matsuo[2], Ikkoh Funaki[3]
[1]Nagoya University
Furo-cho, Chikusa-ku, Nagoya, Japan
[2]Keio University
Hiyoshi, Kohoku-ku, Yokohama, Japan
[3]JAXA Institute of Space and Aeronautical Science
Yoshinodai, Chuo-ku, Sagamihara, Japan

1 Introduction

A detonation wave is a supersonic combustion wave that propagates through reactants with a shock wave [1]. The thermal efficiency and thrust performance using a heat cycle of the detonation combustion are higher than those of conventional constant pressure combustion because the shock wave compresses reactants and increases their temperature and pressure [2,3]. One of the combustors using detonation is the rotating detonation combustor (RDC), in which detonation waves continuously propagate along the combustion chamber wall. Recently, a cylindrical rotating detonation combustor (cylindrical RDC) with a shape similar to conventional combustors was developed [4-6]. Cylindrical RDCs have been actively studied around the world because they can easily incorporate the advantages of detonation into the conventional combustors [4-6].

However, there are some challenges for practical use of RDCs. One of them is the application of liquid propellants. Many combustors, such as thermal power plant combustors, aircraft combustors and rocket combustors, use liquid fuels and liquid oxidizers because of their energy density. In particular, for the application of cylindrical RDCs to rocket combustors, it is essential to verify the applicability of cryogenic propellants, which are widely used in first stage rocket combustors [7]. However, most of the RDC studies with liquid propellants have been conducted with ambient temperature or hypergolic propellants [8,9], and only a few experimental studies have been conducted with cryogenic liquid propellants [10]. In this study, we developed a cylindrical RDC using liquid oxygen, which is a typical cryogenic liquid oxidizer, and investigated the thrust performance.

Correspondence to: ito.shiro.d5@s.mail.nagoya-u.ac.jp

2 Experimental Setup

Figure 1 shows a schematic diagram of the experimental system used in this study. Gaseous ethylene was used as the fuel and liquid oxygen as the oxidizer. Oxygen was supplied directly from an oxygen liquid gas container (LGC). Pressure was measured at three points in the oxygen supply system: p_1: pressure upstream of globe valve 1, p_2: pressure between globe valve 1 and globe valve 2; p_3: pressure downstream of globe valve 2. The pressure sensor (KELLAR Piezoresistive Transmitter: PAA-23) was located 300 mm above the measurement point and measured the pressure of the vaporized oxygen. The temperature upstream of the globe valve 1: T_1 was measured by a T-type thermocouple (Yamari Industries: THERMIC T/SUS316L). The mass flow rate of oxygen was calculated under the assumption that the mass flow rate through the globe valves 1 and 2 is equal to the mass flow rate supplied to the cylindrical RDC combustion chamber. It is also assumed that all oxygen passing through the globe valves is liquid and incompressible. The mass flow rate of gaseous ethylene was determined, assuming that the flow stagnates at the manifold and chokes at the injector outlet. The combustion test was conducted in a vacuum chamber with a volume of 30.1 m^3, and the thrust was measured by a load cell (AIKOH DUD-50K, rating capacity: 500 N). A high-speed camera (Phantom v2011; frame time: 2.3 μs; exposure: 0.38 μs) was used to capture self-luminescence in the combustor through the cylindrical RDC axial direction window on the vacuum chamber. A video camera (GoPro Hero 5) was also used to capture the exhaust plume from the side of the combustor.

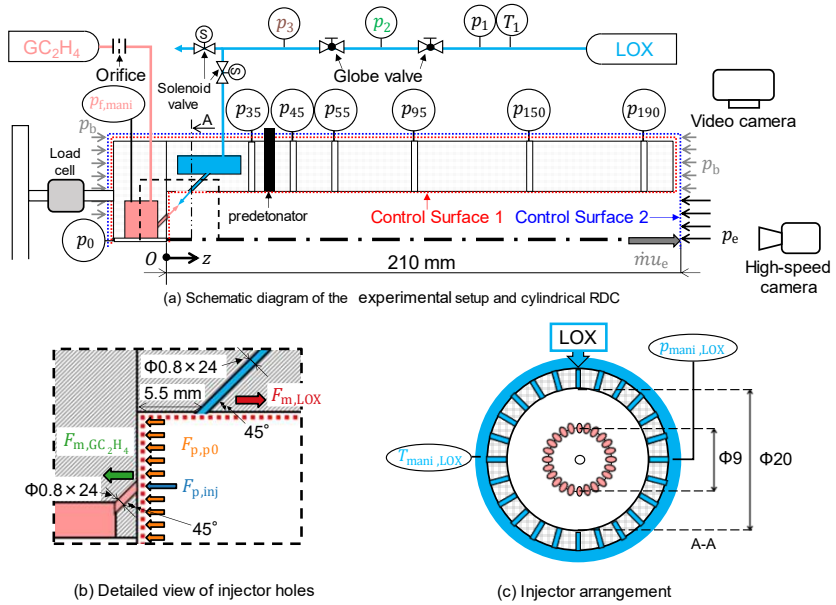

Figure 1: Schematic diagram of the experimental setup

Figure 1 also shows a schematic diagram of the cylindrical RDC. The diameter and axial length of the cylindrical RDC are 20 mm and 210 mm, respectively (Figure 1(a)). As shown in Figure 1(b) and (c), the gaseous ethylene injector (24×ϕ0.8 mm) is located at the bottom of the combustion chamber, while the liquid oxygen injector (24×ϕ0.8 mm) is located on the side wall 5.5 mm from the bottom of the combustion chamber, and each injector is designed to collide with the other's jet at an angle of 180º. Pressure was measured at the ethylene manifold as $p_{\mathrm{f,mani}}$, the oxygen manifold as $p_{\mathrm{ox,mani}}$and the combustion chamber wall asp_z ($z = 0, 35, 45, 55, 95, 150, 190$ mm, p_0 to p_{190}). Temperature was measured in the oxygen manifold as the fluid temperature $T_{\mathrm{ox,mani}}$. The mixture in the cylindrical RDC was ignited by a pre-detonator, in which gaseous ethylene was used as fuel and gaseous oxygen as oxidizer. The pre-detonator port was located at $z = 40$ mm.

3 Results and Discussion

Table 1: Experimental conditions and summary of results

Test No.	$\dot{m}$ [g/s]	ϕ [-]	p_b [kPaA]	F [N]	I_{sp} [s]
1	35 ± 1	1.5 ± 0.1	17 ± 1	54 ± 4	157 ± 12
2	35 ± 1	2.0 ± 0.1	18 ± 1	71 ± 6	204 ± 18
3	36 ± 1	1.8 ± 0.1	18 ± 1	57 ± 4	162 ± 11
4	38 ± 1	1.2 ± 0.1	17 ± 1	75 ± 4	203 ± 10
5	45 ± 1	2.0 ± 0.1	21 ± 1	96 ± 9	217 ± 21
6	53 ± 1	2.2 ± 0.1	23 ± 1	103 ± 9	196 ± 17

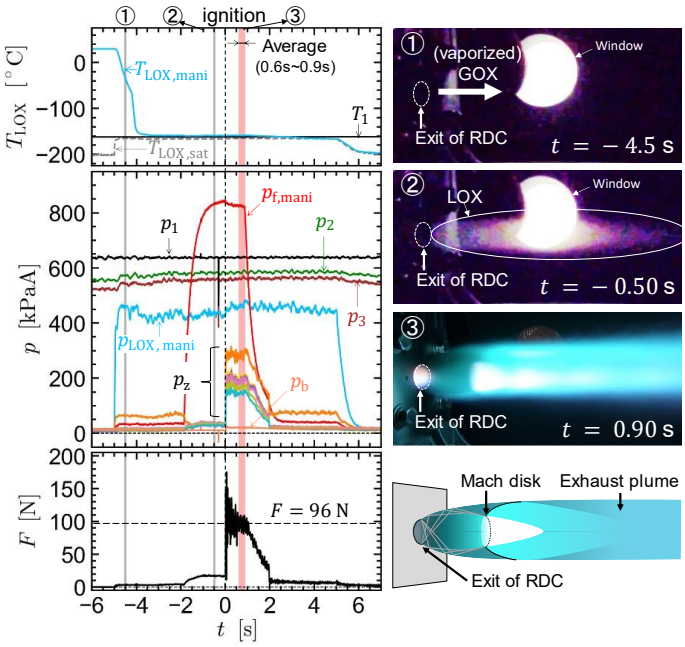

Figure 2: Time variation of temperature(a), pressure(b), thrust(c) and video camera images at the exit of the cylindrical RDC (d)(e)(f) and the schematic of the exaust plume in Test 5,

Table 1 shows the total mass flow rate $\dot{m}$, equivalence ratio ϕ, back pressure p_b, thrust F, and specific impulse I_{sp} of the experiment; all these parameters are the average values from 0.6-0.9 s, which are time from ignition as shown in Figure 2(a), (b) and (c).

3.1 Liquid oxygen supply to the RDC

Figure 2 shows the time variation of temperature (a), pressure (b), and thrust (c) in Test 4 and the images taken by the video camera at the side of the cylindrical RDC at $t = -4.5$ s (d), $t = -0.50$ s (e), and $t = 0.90$ s (f). At $t = -4.5$ s, just after the start of the liquid oxygen supply, the liquid oxygen evaporated and was injected as gaseous oxygen, but at $t = -0.50$ s, just before ignition, the video camera captured the scattered light from the liquid particles, indicating that liquid oxygen was supplied to the cylindrical RDC combustion chamber.

3.2 Rotating detonation waves in the RDC

Figure 3(a) shows images taken by the high-speed camera from the exhaust direction in Test 5; the time interval between each image and the next is 4.65 μs. In all images of Figure 3(a), two high-luminescence areas are seen, and they rotate clockwise. Note that the images have been processed to show the rotation of high-luminescence areas clearly. In order to determine the propagation speed of the rotating high-luminescence areas, a $\theta - t$ diagram was created from the high-speed camera images as shown in Figure 3(b). In the $\theta - t$ diagram, $\theta = 0°$ in the 3 o'clock direction and clockwise is positive. Figure 3(b) shows that the high-luminescence areas propagate at a constant angular velocity, and the propagation velocity is 1383 ± 80 m/s, assuming that the radius of the rotation is equal to the combustion chamber radius of 10 mm. This result suggests that rotating detonation occurred in the combustion test.

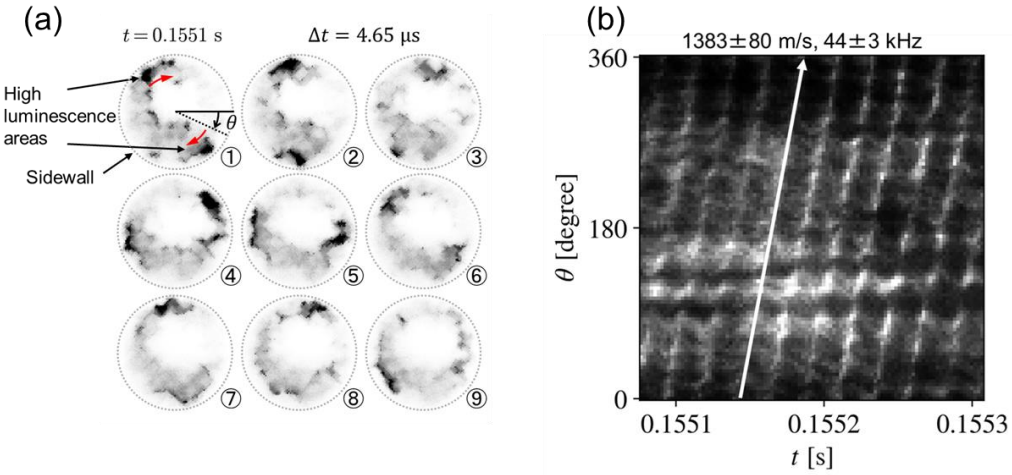

Figure 3: (a) Axial images of two high luminescence areas rotating clockwise in the cylindrical RDC in Test 5 (b) theta-t diagram in Test 5

3.3 Thrust performance

Figure 4 shows the relationship between the mass flow rate and thrust. The plots show the load cell thrust of each experiment. The combustion mode was classified into a detonation mode (round symbol) and a deflagration mode (triangular symbol) according to the type of symbol. The bar graph in Figure 4 shows the thrust F_{cs1} calculated by the following equations (4)-(6) when the control surface is set as Control Surface 1 in Figure 1(a).

$$F_{\mathrm{cs1}} = F_{\mathrm{m}} + F_{\mathrm{p}} \tag{4}$$

$$F_{\mathrm{m}} = F_{\mathrm{m,f}} + F_{\mathrm{m,ox}} = \dot{m}_{\mathrm{m,f}} u_{\mathrm{m,f}} \cos 45° + \dot{m}_{\mathrm{ox}} u_{\mathrm{ox}} \cos 135° \tag{5}$$

$$F_{\mathrm{p}} = F_{\mathrm{p,inj}} + F_{\mathrm{p,p0}} = \left(p_{\mathrm{f,inj}} - p_{\mathrm{b}}\right) \frac{A_{\mathrm{inj,f}}}{\cos 45°} + \left(p_0 - p_{\mathrm{b}}\right) \left(A_{\mathrm{c}} - \frac{A_{\mathrm{inj,f}}}{\cos 45°}\right) \tag{6}$$

$F_{\mathrm{m,f}}$ and $F_{\mathrm{m,ox}}$ in equation (5) are the thrust due to the momentum of ethylene and oxygen jet from the injector into the control volume, respectively, and $F_{\mathrm{p,inj}}$ and $F_{\mathrm{p,p0}}$ in equation (6) are the thrust due to the pressure applied to the ethylene injector outlet surface and the rest of the combustion chamber bottom, respectively. The ethylene injector outlet pressure $p_{p,\mathrm{inj}}$, ethylene injection velocity $u_{\mathrm{f,inj}}$, and oxygen injection velocity $u_{\mathrm{ox,inj}}$, which are necessary for the calculation of equations (5) and (6), are calculated,

assuming that the gaseous ethylene and liquid oxygen stagnating in each manifold are injected isentropically.

The dashed lines in Figure 4 are the thrust F_{cs2} calculated by equation (12) when the control surface is set as Control Surface 2 in Figure 1(a).

$$F_{cs2} = \dot{m}u_e + (p_e - p_b)A_c \tag{12}$$

The exhaust velocity u_e and the pressure at the exit p_e are computed by the following method in each test. The equilibrium of the constant enthalpy and pressure combustion was computed using the temperature of ethylene and oxygen, the combustion pressure and the equivalence ratio as inputs, assuming that the ethylene temperature is equal to the ambient temperature and the oxygen temperature is equal to the boiling temperature at the oxygen manifold pressure. The equilibrium was computed using Python environment running Cantera with the GRI 3.0 mechanism [11,12]. Then, u_e and p_e in equilibrium are computed, assuming that the stagnant burned gas is isentropically accelerated to the sonic velocity and exhausted. The dashed line in Figure 4 plots the relationship between the mass flow rate and thrusts computed by varying the combustion pressure for the experimental conditions of each test. These computed thrusts are equal to the theoretical thrusts for a constant pressure combustion rocket engine of the same geometry.

In Figure 4, the difference between $F_{loadcell}$ and F_{cs1} is within 10% in all tests, suggesting that the measured thrust values are reasonable. The difference between $F_{loadcell}$ and F_{cs2} is also within 10%, except in Test 1 and Test 3, and thus it can be said that $F_{loadcell}$ and F_{cs2} are approximately the same under the limited conditions. This result is consistent with a previous study using gaseous propellants [4], suggesting that the theory of constant pressure combustion rockets can be used to predict thrust performance [13] even when the propellant contains a liquid and additional processes such as atomization and evaporation are involved. Furthermore, the fact that the experimentally measured thrust is almost equal to the theoretical thrust based on the equilibrium calculations suggests that the liquid oxygen reacts completely.

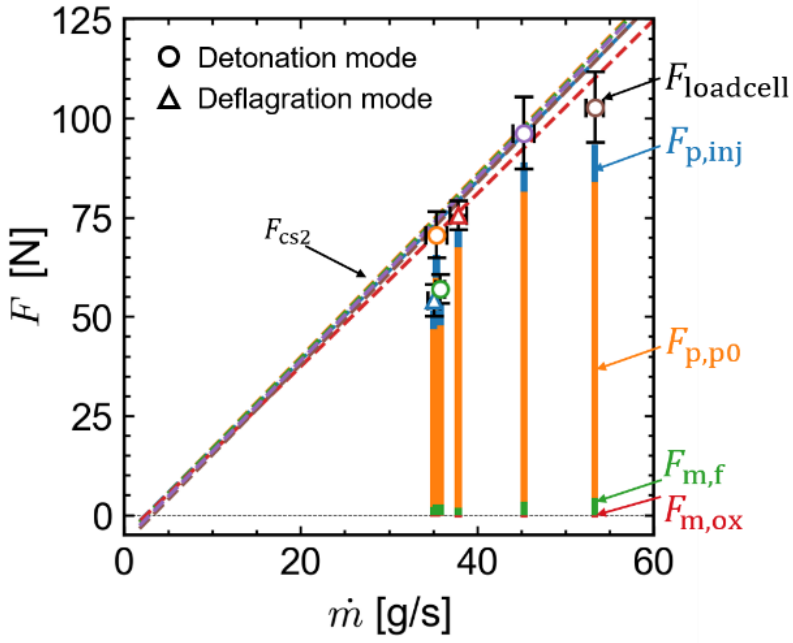

Figure 4 Comparison of the three types of thrust: $F_{loadcell}$ (plots), F_{cs1} (bar plots) and F_{cs2} (dashed lines).

4 Conclusion

Combustion tests were conducted using gaseous ethylene and liquid oxygen in a cylindrical rotating detonation combustor with a diameter of 20 mm and a combustor length of 210 mm. A high-speed camera captures high-luminescence areas rotating along the combustion chamber wall, with a propagation velocity of 1383 ± 80 m/s. This indicates that rotating detonation occurred in the combustion test.

The thrust measured by the load cell F_{loadcell} was in good agreement with the two types of theoretical thrust F_{cs1} and F_{cs2}. F_{cs1} was calculated based on the pressure and momentum exchange, and thus the agreement of F_{loadcell} and F_{cs1}validated the thrust measurement. F_{cs2} was computed based on the equilibrium calculation and the assumption that the exhaust velocity was sonic. The agreement of F_{loadcell} and F_{cs2} suggested that the liquid oxygen reacts completely and that the thrust performance of cylindrical RDCs using liquid propellants can be predicted by the same method as used for the conventional constant pressure combustion rocket engines.

References

[1] Lee JHS. (2008). The Detonation Phenomenon. Cambridge University Press. Cambridge

[2] Zeldovich YB. (2006). Journal of Propulsion Power. Vol.22, No. 3, pp. 588-592

[3] Wolanski P. (2013). Detonative Propulsion. Proc. Combust. Inst. Vol. 34, No. 1, 2013, pp. 125–158.

[4] Yokoo R, Goto K, Kim J, Kawasaki A, Matsuoka K, Kasahara J, Matsuo A, Funaki I. (2020). Propulsion performance of cylindrical rotating detonation engine. AIAA Journal 58, 12, 5107-5116.

[5] Lin W, Zhou J, Liu S, Lin Z. (2015). An Experimental Study on CH4/O2 Continuously Rotating Detonation Wave in a Hollow Combustion Chamber, Experimental Thermal and Fluid Science, Vol. 62, pp. 122-130. doi: 10.1016/j.expthermflusci.2014.11.017

[6] Anand V, George ASt, Gutmark E. (2018). Rotating detonation wave mechanics through ethylene-air mixtures in hollow combustors, and implications to high frequency combustion instabilities, Experimental Thermal and Fluid Science 92, 314-325.

[7] Huzel DK, Huang DH. Modern engineering for design of liquid-propellant rocket engines. Vol. 147. AIAA, Chap. 1, pp. 1–22.

[8] Kindracki J. (2015). Experimental research on rotating detonation in liquid fuel-gaseous air mixtures. Aerospace Science and Technology 43. 445-453.

[9] Anderson WS, Heister SD, Kan B, Hartsfield C. (2020). Experimental study of a hypergolically ignited liquid bipropellant rotating detonation rocket engine. Journal of Propulsion and Power. Vol. 36. No. 6. pp. 851-861.

[10] Bykovskii FA, Zhdan SA, Vedemikov EF. (2006). Continuous Spin Detonations, Journal of Propulsion and Power.Vol. 22, No. 6, 2006, pp. 1204–1216.

[11] Goodwin DG, Speth RL, Moffat HK, Weber BW. (2021). Cantera: An Object-Oriented Software Toolkit for Chemical Kinetics, Thermodynamics, and Transport Processes. Ver. 2.5.1.

[12] Smith GP, Golden DM, Frenklach M, Eiteener B, Goldenberg M, Bowman CT, Hanson RK, Gardiner WC, Lissianski VV, Qin ZW. (2015). GRI-Mech 3.0. Berkeley Mechanical Engineering.

[13] Gordon S, McBride BJ. (1996). Computer Program for Calculation of Complex Chemical Equilibrium Compositions and Applications. NASA RP-1311.